Role of Charged Particle Inertia in Pulsed Electrical Discharges

Jonathan Poggie*

Air Force Research Laboratory, Wright-Patterson AFB, Ohio

In order to investigate the role of inertia in pulsed electrical discharges, this paper compares a five-moment model (continuity, momentum, and energy equations) to a two-moment model (continuity and energy equations) for charged particle motion. Three species were considered: ions, electrons, and neutrals. Either the two- or five-moment model was used for the ions and electrons, but the five-moment model was always employed for the neutrals. Ionization and excitation reactions were included in each model. Two glow discharge test cases in 107 Pa (0.8 Torr) argon were examined. A steady-state, one-dimensional discharge was considered first. For this case, relatively subtle differences in the velocities and temperatures in the cathode sheath led to significant differences between the predictions of the two models for ionization rates and number densities. A two-dimensional, transient discharge problem with an elliptical cathode was studied next. Relative to the two-moment model, the five-moment model predicted a slower response to the activation of the cathode, and lower electron velocities and temperatures in the later stages of the simulation. These differences can be attributed to particle inertia and to differences in the boundary conditions for the two models. Both models predicted that neutral gas velocities on the order of 1.3 m/s occurred within 1000 ns, with a negligible rise in neutral temperature (~ 0.3 K). More rapid heating is expected to occur in molecular gases, which will be the subject of future work.

I. Introduction

This paper examines the role of charged particle inertia in pulsed electrical discharges. Repetitive, short-pulse discharges are a well-known and appealing method for generating ionization and high instantaneous electric fields.[1,2] In aerospace applications, nanosecond-pulse discharges are an emerging tool for plasma-based flow control actuators,[3–5] and have been used as a source of ionization for nonequilibrium magnetohydrodynamic devices.[6,7]

Numerical studies of these discharges are motivated by the need to understand and optimize them. Particle methods, although they provide valuable insight and encompass the greatest portion of the relevant physics, are too computationally costly for practical discharge computations at relatively high pressures.[8] Direct solutions to the Boltzmann equation are also prohibitively costly. The only viable alternatives are continuum models, based on moments of the Boltzmann equation.

Traditional continuum modeling of electrical discharges employs a one-moment model, the continuity equation, with particle transport properties and ionization rates taken as a function of the reduced electric field.[9–11] More recent studies have extended this model by substituting an electron energy equation in place of the reduced electric field dependence.[12–14] Only a few studies have considered particle inertia; these typically have assumed constant ion temperature.[15–18]

Even though traditional continuum discharge models are useful for predicting particle densities in industrial plasma processing applications,[1,2] they may not be suitable for discharges used for aerospace applications, where the intent is to transfer momentum and energy from the charged particles to the neutrals in order to modify the flow. Further, many of the assumptions typically employed in these models may not be suitable for pulsed discharges.

*Senior Aerospace Engineer, Associate Fellow AIAA.

Cleared for public release, distribution unlimited (88ABW-2009-4977).

In particular, the full set of Maxwell's Equations may have to be solved, charged particle inertia may be a significant effect, and local charged particle temperatures may not reflect a local equilibrium with the electric field. This paper addresses the latter two issues, comparing a five-moment model for the charged particles to a two-moment model. (It should be noted that coupling of fluid models to the full Maxwell's Equations has been treated by other researchers,[19,20] and that that two-fluid, five-moment models have been employed in the fusion plasma community,[21] but typically for a weakly-collisional regime.)

Here the temperature variation of ions, electrons, and neutrals is considered, and a model incorporating continuity, momentum, and energy equations for each species is compared to one that replaces the momentum equation with the drift-diffusion approximation. The simpler model will be called the two-moment model (continuity and energy). Although the calculations presented here are at most two-dimensional, the more general model will be called the five-moment model (continuity, three momentum components, and energy) for consistency with the literature.

II. Physical Model

This section will outline the two physical models employed in this work. Both are based on moments of the Boltzmann equation, and an outline of their derivation is given in Appendix A. The working gas was taken to be argon for all the test cases considered in this paper.

A. Five-Moment Model

First we discuss the five-moment model, which includes particle inertia. The conservation equations for each species are:

$$\begin{aligned}
\frac{\partial}{\partial t}\left(m_s n_s\right) + \nabla\cdot\left(m_s n_s \mathbf{v}_s\right) &= S_s \\
\frac{\partial}{\partial t}\left(m_s n_s \mathbf{v}_s\right) + \nabla\cdot\left(m_s n_s \mathbf{v}_s\mathbf{v}_s + p_s\mathbf{I}\right) &= \nabla\cdot\tau_s + q_s n_s \mathbf{E} + \mathbf{A}_s \\
\frac{\partial}{\partial t}\left[m_s n_s\left(\epsilon_s + \tfrac{1}{2}v_s^2\right)\right] + \nabla\cdot\left[m_s n_s \mathbf{v}_s\left(\epsilon_s + \tfrac{1}{2}v_s^2\right) + p_s\mathbf{v}_s\right] &= \nabla\cdot\left[\tau_s\cdot\mathbf{v}_s - \mathbf{Q}_s\right] + q_s n_s \mathbf{v}_s\cdot\mathbf{E} + M_s
\end{aligned} \tag{1}$$

where the notation $s = i, e, n$ indicates the ions, electrons, and neutrals, respectively.

The mass per particle of each species is denoted as m_s, and the corresponding charge per particle is $q_{i,e} = \pm e$ and $q_n = 0$. The number density is n_s, the velocity is $\mathbf{v}_s$, and the translational temperature is T_s. The electric field is $\mathbf{E}$. The pressure is found from $p_s = n_s k_B T_s$, where k_B is the Boltzmann constant. The internal energy per particle is assumed to have the form $m_s\epsilon_s = H_s + k_B T_s/(\gamma_s - 1)$, where $\gamma_s = 5/3$ is the ratio of specific heats and H_s is the heat of formation per particle of species-s.

In order to close the equation set (1), models are needed for the collision source terms S_s, $\mathbf{A}_s$, and M_s, the viscous stress tensor τ_s, and the heat flux vector $\mathbf{Q}_s$. For the inelastic collision terms, the following ionization and excitation reactions were considered:

$$\begin{aligned}
\mathrm{Ar} + \mathrm{e} &\rightarrow \mathrm{Ar}^+ + 2\mathrm{e} \\
\mathrm{Ar} + \mathrm{e} &\rightarrow \mathrm{Ar}^* + \mathrm{e}
\end{aligned}$$

The reaction rates were taken from Park and Economou,[22] with the form $\omega_I = k_I n_e n_n$ for the ionization rate, and $\omega_X = k_X n_e n_n$ for the excitation rate. A more complete model would include conservation equations for the excited atoms, but for simplicity, the only effect of excitation considered in the present model was an energy loss from the electrons. Recombination reactions are neglected in the present work.

The inelastic collision components of the collision source terms have the form:

$$\begin{array}{lll}
S_i = m_i\omega_I & \mathbf{A}_i = m_i\omega_I\mathbf{v}_i & M_i = m_i\omega_I(\epsilon_i + \frac{1}{2}v_i^2) \\
S_e = m_e\omega_I & \mathbf{A}_e = m_e\omega_I\mathbf{v}_e & M_e = m_e\omega_I(\epsilon_e + \frac{1}{2}v_e^2) - \omega_I\mathcal{H}_I - \omega_X\mathcal{H}_X \\
S_n = -m_n\omega_I & \mathbf{A}_n = -m_n\omega_I\mathbf{v}_n & M_n = -m_n\omega_I(\epsilon_n + \frac{1}{2}v_n^2)
\end{array} \tag{2}$$

where $\mathcal{H}_I$ is the energy lost by electrons in ionizing collisions, and $\mathcal{H}_X$ is the corresponding energy lost in excitation collisions. For this model, the ions are assumed to appear out of ionizing collisions with the average momentum and energy of their peers. Similarly, the neutrals that are lost to ionization are assumed

to have the same average momentum and energy as the other neutral particles. The electrons, however, lose additional energy because only the most energetic electrons initiate the collisions that cause ionization and excitation. A discussion of the form of the inelastic collision source terms is given in Appendix B.

The momentum and energy source terms also have an elastic collision component. Because the gas is assumed to be weakly ionized, the primary elastic collisions are with neutral particles. The form of the elastic collision term is taken from Burgers,[23] and is discussed in Appendix C. In this model, the momentum and energy source terms due to elastic collisions have the form:

$$\begin{aligned} \mathbf{A}_i &= -n_i m_{in}\nu_{in}(\mathbf{v}_i - \mathbf{v}_n) \qquad M_i = -\frac{n_i m_{in}\nu_{in}}{m_i + m_n}\left[3k_B(T_i - T_n) + (\mathbf{v}_i - \mathbf{v}_n)\cdot(m_i\mathbf{v}_i + m_n\mathbf{v}_n)\right] \\ \mathbf{A}_e &= -n_e m_{en}\nu_{en}(\mathbf{v}_e - \mathbf{v}_n) \qquad M_e = -\frac{n_e m_{en}\nu_{en}}{m_e + m_n}\left[3k_B(T_e - T_n) + (\mathbf{v}_e - \mathbf{v}_n)\cdot(m_e\mathbf{v}_e + m_n\mathbf{v}_n)\right] \\ \mathbf{A}_n &= -(\mathbf{A}_i + \mathbf{A}_e) \qquad\qquad\qquad M_n = -(M_i + M_e) \end{aligned} \tag{3}$$

where $m_{sn} = m_s m_n/(m_s + m_n)$ is the reduced mass, with $s = i, e$. The collision frequency between the charged and neutral species ν_{sn} was estimated from mobility data, with the correlations for ion and electron mobility in argon taken from Ward.[9] The overall collision source terms are the sum of the inelastic collision component, Eq. (2), and the elastic collision component, Eq. (3).

For the flux terms, it was assumed that the viscous term had a Newtonian form, with Stokes hypothesis applied, and that the heat flux followed Fourier's law:

$$\begin{aligned} \tau_s &= \mu_{vn}\left[(\nabla\mathbf{v}_s) + (\nabla\mathbf{v}_s)^T - \tfrac{2}{3}\nabla\cdot\mathbf{v}_s\mathbf{I}\right] \\ \mathbf{Q}_s &= -k_s\nabla T_s \end{aligned} \tag{4}$$

where μ_{vs} is the viscosity and k_s is the thermal conductivity for species-s. The properties of the neutrals were taken from standard correlations for argon.[24] The charged particle transport properties were derived from mobility data, assuming a Lewis number of $\mathrm{Le}_s = m_s n_s C_{ps} D_s/k_s = 1$ and a Prandtl number of $\mathrm{Pr}_s = \mu_{vs}C_{ps}/k_s = 2/3$, where D_s is the species diffusion coefficient and $C_{ps} = 5k_B/(2m_s)$ is the specific heat at constant pressure. The results are:

$$\begin{aligned} D_s &= \frac{k_B T_s}{|q_s|}\mu_s \\ \mu_{vs} &= \tfrac{2}{3}n_s m_s D_s \\ k_s &= \tfrac{5}{2}k_B n_s D_s \end{aligned} \tag{5}$$

where $\mu_s = |q_s|/(m_{sn}\nu_{sn})$ is the species mobility. Note that these transport coefficients are proportional to number density, so the electron transport properties become small for the low electron number densities in the cathode sheath.

B. Two-Moment Model

Next we discuss the two-moment model, or drift-diffusion formulation. This model neglects the acceleration terms in the momentum equation, and also neglects all viscous terms. The governing equations are reduced to:

$$\begin{aligned} \frac{\partial}{\partial t}(m_s n_s) + \nabla\cdot(m_s n_s\mathbf{v}_s) &= S_s \\ n_s\mathbf{v}_s = n_s\mathbf{v}_n \pm n_s\mu_s\mathbf{E} - \frac{D_s}{k_B T_s}\nabla p_s & \\ \frac{\partial}{\partial t}(m_s n_s\epsilon_s) + \nabla\cdot(m_s n_s\mathbf{v}_s\epsilon_s) &= -\nabla\cdot\mathbf{Q}_s - p_s\nabla\cdot\mathbf{v}_s + \tilde{M}_s \end{aligned} \tag{6}$$

where the value of the species mobility μ_s was taken from Ward.[9] Note that here we solve the thermal energy equation, obtained by subtracting the mechanical energy equation, the scalar product of $\mathbf{v}_s$ and Eq. (1b), from the total energy equation (1c). The energy source terms are thus slightly different from those in Eqs. (2)-(3), and have the form:

$$\begin{aligned} \tilde{M}_i &= m_i\omega_I\epsilon_i + \frac{n_i|q_i|}{(m_i + m_n)\mu_i}\left[-3k_B(T_i - T_n) + m_n|\mathbf{v}_i - \mathbf{v}_n|^2\right] \\ \tilde{M}_e &= m_e\omega_I\epsilon_e - \omega_I\mathcal{H}_I - \omega_X\mathcal{H}_X + \frac{n_e|q_e|}{(m_e + m_n)\mu_e}\left[-3k_B(T_e - T_n) + m_n|\mathbf{v}_e - \mathbf{v}_n|^2\right] \end{aligned} \tag{7}$$

Note that the velocity difference terms due to elastic collisions are always positive. They have a dissipative nature, always tending to increase the thermal energy.

This two-moment formulation was only used for the charged particles; the neutrals were handled using Eq. (1).

C. One-Moment Model

For completeness, we derive the one-moment model that that corresponds to the formulation used in this paper. The one-moment model employs the continuity equation for each species, along with the drift-diffusion approximation for the particle fluxes. The particle transport properties and ionization rates are taken as a function of the reduced electric field.

The required relation between the electron temperature and reduced electric field can be found by assuming a homogeneous discharge. Considering the electron thermal energy equation (6)c, and neglecting all the terms in that involve gradients of the discharge properties, we obtain $\tilde{M}_e = 0$. Introducing the drift approximation for the electron velocity, and simplifying, we obtain:

$$\left(\frac{E}{n_n}\right)^2 = \frac{3k_B(T_e - T_n)}{m_n(\mu_e n_n)^2} + \frac{k_I\mathcal{H}_I + k_X\mathcal{H}_X}{e(\mu_e n_n)} \tag{8}$$

Given the form of the scaled electron mobility $\mu_e n_n$, the ionization rate k_I, and the excitation rate k_X, this equation provides an implicit relation between the reduced electric field and the electron temperature: $f(E/n_n, T_e) = 0$.

The corresponding model for the ions can be found by setting $\tilde{M}_i = 0$. The resulting equation for the rise in ion temperature is:

$$T_i - T_n = \frac{m_n}{3k_B}(\mu_i n_n)^2 \left(\frac{E}{n_n}\right)^2 \tag{9}$$

D. Poisson Equation

To complete the physical model, the electric field must be found from a consistent solution of Maxwell's equations. For the present work, the Poisson equation was solved for the electric potential:

$$\nabla^2\phi = -\frac{e}{\epsilon_0}(n_i - n_e) \tag{10}$$

and the electric field was found from $E = -\nabla\phi$.

III. Numerical Methods

This section briefly outlines the structure of the flow solver, and goes on to discuss the physical and numerical boundary conditions.

A. Flow Solver

In transformed coordinates, the two-dimensional forms of the conservation laws (1) and (6) can be written in the form:

$$\frac{\partial U}{\partial t} + \frac{\partial E}{\partial \xi} + \frac{\partial F}{\partial \eta} = \frac{\partial E_v}{\partial \xi} + \frac{\partial F_v}{\partial \eta} + S \tag{11}$$

where U is the vector of conserved variables, E and F are the inviscid flux vectors, E_v and F_v are the viscous flux vectors, and S represents the source terms. A standard, low-storage, fourth-order Runge-Kutta scheme[25] was used for time integration of Eq. (11).

Spatial differencing was carried out with the Steger-Warming flux splitting scheme for the five-moment model, and with a simple scalar upwind scheme for the two-moment model. The code employed third-order MUSCL extrapolation[26] for the inviscid fluxes and second-order central differencing for the viscous terms. A harmonic limiter was employed.

The Poisson equation (10) was solved at the end of each stage of the Runge-Kutta time-integration. It can be written in the following form in transformed coordinates:

$$\frac{\partial E}{\partial \xi} + \frac{\partial F}{\partial \eta} = S_\phi \tag{12}$$

An iteration procedure was introduced such that the potential at iteration step m was $\phi^{m+1} = \phi^m + \Delta\phi$. With a linear expansion about the solution from the previous iteration, and approximate factoring of the implicit terms, the discretized equation has the form:

$$\left[1 - \Delta\tau(\delta_\xi A \delta_\xi - D)\right]\left[1 - \Delta\tau \delta_\eta B \delta_\eta\right]\Delta\phi = \omega\Delta\tau\left[\frac{\partial E^m}{\partial \xi} + \frac{\partial F^m}{\partial \eta} - S_\phi^m\right] \tag{13}$$

with iteration driving $\Delta\phi$ to zero. Here A and B are flux Jacobians, D is the source Jacobian, τ is a time-like variable introduced to motivate the iteration process, and ω is an over-relaxation factor. Discretizing the left-hand side using second order central differences in space, a tridiagonal system of equations is obtained. A second-order central difference scheme was also used to evaluate the spatial differences present on the right hand side of Eq. (13), and the system was solved using the Thomas tridiagonal algorithm.[27] The pseudo-time-step $\Delta\tau$ was varied cyclically to accelerate convergence, and iteration was continued until the change in potential $\Delta\phi$ had dropped below a specified tolerance.

B. Boundary Conditions

For the neutral particles, boundary conditions of no-slip ($\mathbf{v}_n = 0$) and no temperature jump ($T_n = T_\infty$) were imposed at solid boundaries. The boundary conditions for the charged particles were based on those of Graves[28] and Wilcoxson and Manousiouthakis,[18] and are summarized for the two physical models in Fig. 1.

The boundary condition on the electron flux at an electrode is set by a balance between recombination and secondary emission: $n_e v_e^\perp = n_e k_r - \gamma_E n_i v_i^+$. Here we use the notation $v^\perp = \mathbf{v}\cdot\mathbf{n}$, where $\mathbf{n}$ is the outward normal, and $v_i^+ = \max(v_i^\perp, 0)$. The symbol γ_E represents the secondary emission coefficient, and k_r is a recombination coefficient with dimensions of velocity. Ion emission is prohibited, and the ion recombination rate at the boundary is assumed to be sufficiently fast to absorb any flux of ions.

For the two-moment model, the flux boundary conditions are imposed by using Eq. (6b) to set the particle pressure to match the boundary condition (Fig. 1c-d). For the five-moment model, the flux boundary conditions are imposed through the velocity, with the restriction that electron emission is limited to sonic speed (Fig. 1a-b). Where an additional boundary condition is required mathematically, the tangential component of velocity ($\mathbf{v}^\parallel = \mathbf{v} - v^\perp\mathbf{n}$) is set to zero.

Electron temperature at the boundary reflects a balance between the population of electrons flowing toward the wall and recombining, and the population emitted from the wall through secondary emission. As a rough model of this process, electron temperature is found from a flux-weighted average of the secondary emission temperature T_{es} and the temperature of the recombining particles T_{ea}:

$$\mathrm{avg}(T_{ea}, T_{es}) = \frac{n_e k_r\, T_{ea} + \gamma_E n_i v_i^+\, T_{es}}{n_e k_r + \gamma_E n_i v_i^+}$$

Here the recombination temperature is estimated from the simplified energy equation $\frac{5}{2}k_B \nabla T_{ea}\cdot\mathbf{n} = -e\mathbf{E}\cdot\mathbf{n}$. The electron recombination rate is evaluated as the thermal speed at the temperature of the wall-directed population: $k_r = \sqrt{k_B T_{ea}/(2\pi m_e)}$.

Where an ion temperature boundary condition was required, it was set to the ambient temperature T_∞. To distinguish between inflow and outflow before applying the boundary conditions, extrapolation of the velocity field was used. (All extrapolation employed second-order accuracy.) The limit of sonic electron emission was enforced as a check after applying the subsonic boundary conditions.

IV. Results

Two test cases were considered. The first was a basic, one-dimensional, DC discharge problem used to verify that the algorithms were implemented correctly. The second was a two-dimensional transient problem, designed to emphasize the differences between to two models.

A. DC Discharge in One Dimension

As a first test case, calculations were carried out with both models for a DC glow discharge in one dimension. The conditions were chosen to be similar to those used by Meyyappan and Kreskovsky.[15] (Those calculations did not include an excitation reaction, viscous terms, or ion temperature variation, so the present calculations are slightly different.)

The background neutral gas (argon) was assumed to be at rest, with a pressure of 107 Pa (0.8 Torr) and temperature of 323 K. The imposed potential was 120 V and the discharge gap was 35.25 mm. The initial condition was taken to be a uniform plasma of number density $n = 10^{15}$ m^{-3}, with temperatures $T_i = 323$ K (0.03 eV) and $T_e = 11600$ K (1 eV). The secondary emission coefficient was $\gamma_E = 0.05$, and the secondary emission temperature was $T_{es} = 5800$ K (0.5 eV). A total of 151 points were used across the discharge gap in the calculations, which were marched in time to 1.0 ms. (It should be noted here that poor grid resolution in the region of peak ionization can lead to run-away ionization for this problem.)

The basic discharge results are shown in Fig. 2. The data are nondimensionalized by the following reference values: $n_0 = 10^{16}$ m^{-3}, $u_R = 1$ km/s, and $L = 35.25$ mm. Number densities and electric potential are shown in Fig. 2a, temperatures in Fig. 2b, velocities in Fig. 2c, and ionization rate in Fig. 2d.

The product of pressure and gap width is $pL = 3.8$ m-Pa (2.8 cm-Torr). The normal cathode fall thickness for argon is given as $pd \approx 0.3$ cm-Torr by Lieberman and Lichtenberg[1] (p. 462), so the cathode layer thickness of $d \sim 0.15L$ seen in Fig. 2a is on the right order.

The electrons emitted from the cathode are initially accelerated by the strong electric field, reaching remarkably high peak velocities ($\sim 10^6$ m/s). Their directed energy is randomized in collision with neutrals, leading to a reduced mean velocity and increased electron temperatures, up to ~ 12 eV. High temperature leads to higher ionization rates, the energy cost of which brings the electron temperature back down to 1-2 eV in the positive column. Electrons are absorbed at the anode.

Ions generated in the center of the domain are absorbed at both boundaries. Ion velocities are substantially higher at the cathode ($\sim$2 km/s), and collisions with neutrals in that region lead to an order of magnitude increase in ion temperature there (up to $\sim$0.5 eV).

The five-moment model and the drift-diffusion model predict similar temperatures (Fig. 2b) and velocities (Fig. 2c) under these conditions. Subtle differences in the results for the two models are magnified, however, by the extreme sensitivity of the ionization rate, leading to greater ionization rates (Fig. 2d) and plasma densities (Fig. 2a) for the two-moment model.

The relative magnitudes of the electron heating terms of Eq. (7b) are shown in Fig. 3. The terms are nondimensionalized in the plot by dividing by $m_n n_0 u_R^3 / L$. The terms are labelled as follows:

Ionization Cost:	$-\omega_I \mathcal{H}_I$
Excitation Cost:	$-\omega_X \mathcal{H}_X$
Temperature Equilibration:	$-\frac{n_e \lvert q_e \rvert}{(m_e+m_n)\mu_e} 3k_B(T_e - T_n)$
Frictional Dissipation:	$\frac{n_e \lvert q_e \rvert}{(m_e+m_n)\mu_e} m_n \lvert \mathbf{v}_e - \mathbf{v}_n \rvert^2$

with their sum labeled 'Total Heating.'

Although there are quantitative differences between the predictions of the two models, the results are qualitatively the same. The frictional dissipation term adds heat to the system, and is balanced by the other terms, which represent thermal energy losses. The double-peaked profile of ionization cost mirrors the ionization profiles shown in Fig. 2d. The excitation cost also shows a double-peaked profile, with the relative magnitudes of the two peaks reversed relative to the ionization term. The temperature equilibration term is not significant in the cathode layer, but plays an important role in limiting electron temperatures in the positive column.

The corresponding ion heating terms of Eq. (7a) reflect a close balance between the frictional dissipation and the temperature equilibration terms, for a moderate net heating rate. (The corresponding plots are omitted for brevity.) Peak values of these terms occur near the cathode.

The results obtained here are qualitatively similar to those of Meyyappan and Kreskovsky[15] for the same conditions. (The present model includes viscous terms, ion temperature variation, and excitation reactions, which were omitted by Meyyappan and Kreskovsky.) Those authors observed similar number density distributions, although with very low densities in the cathode layer. They also obtained a similar ionization profile, with two peaks, the larger being the closer to the cathode. Their electron temperature and velocity profiles also showed large peaks in the cathode layer.

B. Transient Discharge with Elliptical Cathode

The second test case was designed to highlight the differences between the two- and five-moment models. It is a two-dimensional, transient problem, where particle inertia, electric field strength, and charged particle heating could be expected to be significant.

A schematic diagram of the problem is given in Fig. 4a. The inner boundary is taken to be the cathode, which is brought suddenly to a potential of $\phi = -120$ V at $t = 0$. The shape of the cathode is a 4:1 ellipse, and the grounded anode forms the circular outer boundary.

The 101×101 point computational grid is shown in Fig. 4b. It is an O-grid, with five-point overlap at the cut on the positive x-axis. (The overlap region is indicated by red lines in the figure.) An initial grid was generated algebraically, with clustering near the tips of the ellipse and at the inner and outer boundaries. This grid was then smoothed and made close to orthogonal using the commercial grid manipulation program Gridgen, from Pointwise, Inc. The minimum gap between the inner and outer electrodes was taken to be 35.25 mm to match the previous test case.

The initial and boundary conditions were also similar to those used in the previous test case. The background neutral gas was at initially at rest at 107 Pa and 323 K. A uniform plasma of number density $n = 10^{15}$ m^{-3}, with temperatures $T_i = 323$ K (0.03 eV) and $T_e = 11600$ K (1 eV), was assumed to exist at $t = 0$ between the two electrodes. Again, the secondary emission coefficient was $\gamma_E = 0.05$, and the secondary emission temperature was $T_{es} = 5800$ K (0.5 eV).

To highlight the initial evolution of the cathode sheath, Figs. 5-8 show the region around the right tip of the cathode for times of 1, 10, 100, and 1000 ns. In the number density distributions shown in Figs. 5a, 6a, 7a, and 8a, the sheath is seen to gradually thicken and the number densities to increase rapidly due to ionization. Looking at the electric potential distribution as a function of time, we see the rapid development of a strong electric field near the cathode (compare Figs. 5b, 6b, 7b, and 8b).

There is a corresponding increase in ion and electron temperature near the cathode (Figs. 5c, 6c, 7c, and 8c). Note the local maximum in electron temperature between $0.2L \leq x \leq 0.22L$; it is starting to form at $t = 1$ ns and is quite prominent at $t = 10$ ns. This peak grows rapidly with time. Ion temperature is seen to peak at the cathode surface.

The distributions of the horizontal component of velocity have an analogous form: the ion velocity peaks at the cathode, whereas the electron velocity has a local maximum some distance away from the wall. It is interesting to note that the electrons initially flow into the cathode, where they are absorbed through recombination (Fig. 5d), but as the ion bombardment of the cathode increases, the secondary emission rate exceeds the recombination rate and there is a net outflow of electrons as (Fig. 6d).

Corresponding results for the neutral particles are shown in Fig. 9. The neutrals are slower to respond to initiation of the discharge. At $t = 10$ ns, the neutral velocity is about 0.05 m/s, directed toward the cathode tip, and the neutral temperature is essentially unchanged. By $t = 1000$ ns, the neutral velocity has increased to about 1.3 m/s, and the neutral temperature has risen very slightly (about 0.3 K). For the neutral gas properties, the predictions of the two physical models are essentially the same. (Recall that the five-moment model was always used for the neutrals in this work; only the model for the charged particles was changed.)

Significant differences, however, are observed between the predictions of the two models for the charged particles in the initial stages of the development of the cathode sheath (Figs. 5-8). Although the results have qualitative similarity, the response of the five-moment model to the suddenly-applied potential is slower than that of the two-moment model. In particular, the local maxima in electron temperature and velocity are lower for the five-moment model than for the two-moment model, as are the corresponding maxima for the ions at the cathode surface. By $t = 1000$ ns, the predicted ion properties are very close for the two models, but significant differences remain for the electrons (Fig. 7).

Although it is difficult to represent in printed form, the results from the five-moment model, observed in flowfield movies, show acoustic waves propagating through the domain during the initial transient. These waves are not captured with the two-moment model.

Figures 10-11 show the two-dimensional property fields at $t = 1000$ ns for the five- and two-moment models, respectively. Particle number densities are shown in Figs. 10a and 11a, where the color contours represent the ions and the black lines the electrons. The electron-free sheath is apparent in the plots, as is a ring of high plasma density just outside the sheath.

Figures 10b-f and 11b-f show a field of view close in around the cathode. The potential distribution illustrates the strong electric field and large potential drop in the cathode sheath (Figs. 10b and 11b). Peak ion temperatures occur at the tips of the cathode (Figs. 10c and 11c), whereas the peak electron temperature

appears as a ring around the cathode (Figs. 10d and 11d). Peak charged particle speed is also seen to occur at the tips of the cathode (Figs. 10e-f and 11e-f).

As mentioned above, the results of the five-moment model tend to lag those of the the two-moment model because of the effects of inertia. Thus the temperatures and velocities are generally lower for the five-moment model (Fig. 10) than for the two-moment model (Fig. 11).

Corresponding results for the neutral particles are shown in Fig. 12. The features of the neutral particle fields are similar to those for the ions, with peak temperatures near the cathode tips, and significant inflow velocity there. These results reflect elastic collisions between ions and neutrals.

V. Summary and Conclusions

In order to investigate the role of inertia in pulsed electrical discharges, this paper compared a five-moment model (continuity, momentum, and energy equations) to a two-moment model (continuity and energy equations) for charged particle motion. Three species were considered: ions, electrons, and neutrals. Either the two- or five-moment model was used for the ions and electrons, but the five-moment model was always employed for the neutrals. Ionization and excitation reactions were included in each model.

Two glow discharge test cases in 107 Pa argon were examined. The first was a basic, one-dimensional, DC discharge problem used to verify that the algorithms were implemented correctly. The basic results were found to be in qualitative agreement with those of Meyyappan and Kreskovsky.[15] Electron temperature and velocity profiles showed large local maxima in the cathode layer, whereas the corresponding ion properties peaked at the cathode. Two peaks were observed in the ionization profile, with the larger closer to the cathode. Fine grid resolution was required near these peaks to obtain acceptable numerical solutions. Comparing the results from the two- and five-moment models, it was observed that subtle differences in the velocities and temperatures in the cathode sheath led to significant differences between the predictions of the two models for ionization rates and number densities.

The second test case was a two-dimensional transient problem with an elliptical cathode, designed to emphasize the differences between the two models. Relative to the two-moment model, the five-moment model predicted a slower response to the activation of the cathode, and predicted acoustic waves propagating through the domain. In particular, the development of the charged particle temperature and velocity distributions for the five-moment model lagged that for the two-moment model. By 1000 ns, the ion properties had nearly caught up, but substantial differences remained for the electron properties. These differences can be attributed to the effects of particle inertia and to differences in the boundary conditions for the two models.

The evolution of the properties of the neutrals was also studied for this problem. Both models predicted that neutral gas velocities on the order of 1.3 m/s occurred within 1000 ns, with a negligible rise in neutral temperature (~ 0.3 K). The slow temperature rise may be a feature of the monatomic gas, argon, considered in this study. In molecular gases, the fastest energy transfer path from the electrons to the neutrals is molecular dissociation into high-energy products through electron impact.[3] For pulsed discharges in air on the order of 10 ns in duration, an overheating on the order of 100 K has been obtained experimentally[3] within 1000 ns. To study flow control actuators, therefore, it will be necessary to move to a reasonably realistic model for air; discharges in molecular gases are a topic of ongoing work.

In summary, calculations with the five-moment model are seen to be feasible, and may prove to be a useful tool in studying nanosecond-pulse discharges. The computational cost for the five-moment model is about twice that of the two-moment model, as based on timings of the two-dimensional calculations presented here. Since significant differences in the charged particle behavior are observed between the two models, the increased generality of the five-moment model may be worth the additional computational cost.

Appendix A: A Short Derivation of the Moment Equations

A brief discussion is presented here on the derivation of the conservation laws as moments of the Boltzmann equation. Useful references for additional details include Chapman and Cowling,[29] Seshadri,[30] and Olejniczak and Candler.[31]

Starting from the molecular dynamics viewpoint, classical Newtonian mechanics is assumed to hold, and

the particle acceleration $\mathbf{a}$ is assumed to be generated by gravity and the Lorentz force:

$$m_s\mathbf{a} = m_s\mathbf{g} + q_s\left(\mathbf{E} + \mathbf{u}\times\mathbf{B}\right) \tag{14}$$

Here m_s is the mass per particle, $\mathbf{g}$ is the acceleration due to gravity, q_s is the electric charge per particle, $\mathbf{u}$ is the particle velocity, $\mathbf{E}$ is the electric field, and $\mathbf{B}$ is the magnetic field.

The state of a particle can be specified by its position and velocity, the phase-space coordinates $(\mathbf{x}, \mathbf{u})$. In principal, the motion of a large group of particles can be predicted from Eq. (14), given all their positions and velocities at a certain time. In practice, this is not possible because of computational cost and sensitivity to initial conditions. Therefore, we are driven to describe the physics statistically, predicting macroscopic quantities, averaged over a large number of particles.

The fundamental dependent variable from the statistical point of view is the velocity distribution function for species-s, $f_s(\mathbf{x}, \mathbf{u}, t)$, which represents the probability of finding a particle in a particular small element of phase space. Here it is normalized so that the integral over all velocity space is unity:

$$\int f_s(\mathbf{x}, \mathbf{u}, t)\, d^3u = 1 \tag{15}$$

This definition requires that the distribution function tend to zero as the velocity components become large.

In the statistical treatment that follows, the electric and magnetic fields in Eq. (14) are taken to be macroscopic fields, obtained by averaging over a volume large enough to contain a large number of particles, but small compared to the length scale of macroscopic property variations. Particle trajectories are assumed to be governed by Eq. (14), except during collisions where the motion is governed by intermolecular forces (and where quantum mechanical effects may be significant). The gas is also assumed to be sufficiently dilute that these collisions can be considered as rare, discrete, short-duration events.

With these assumptions, and the restriction that a statistically significant number of particles be present in the small volume under consideration, the generalized Boltzmann equation, or equation of change of the probability density function, can be written as:

$$\frac{\partial}{\partial t}(n_s f_s) + \mathbf{u}\cdot\nabla(n_s f_s) + \mathbf{a}\cdot\nabla_u(n_s f_s) = \omega_s \tag{16}$$

The independent variables are particle velocity $\mathbf{u}$, position $\mathbf{x}$, and time t. Here n_s is the number density and ω_s represents the particle production rate due to collisions. (A derivation of the Boltzmann equation from the Liouville Theorem can be found in Ch. 7 of Hirschfelder, Curtis, and Bird.[32])

Equation (16) can be interpreted as stating that the number of particles observed, while following a selected initial group along their trajectories in phase space, is altered only by their sudden appearance or disappearance in local phase space through collisions. Given a suitable collision model, it can be solved to find the time-evolution of the distribution function. In a gas mixture, there is a Boltzmann equation for each species present; they are coupled through the collision term ω_s.

Other statistical quantities of interest are average values, which are more readily-measured, macroscopic properties. Considering a quantity $\phi(\mathbf{u})$ associated with each particle, an average value is defined as:

$$\langle\phi\rangle_s(\mathbf{x}, t) = \int \phi(\mathbf{u}) f_s(\mathbf{x}, \mathbf{u}, t)\, d^3u \tag{17}$$

where the integral is over all velocity space. Equations for the evolution of average values can be obtained from moments of the Boltzmann equation.

To obtain a moment equation, Eq. (16) is multiplied by ϕ, and integrated over all velocity space. It is assumed that, as the magnitude of the velocity approaches infinity, the velocity distribution function approaches zero sufficiently rapidly that the required moments of the velocity converge. The resulting equation of change of $\langle\phi\rangle_s$, or the transport equation, is:

$$\frac{\partial}{\partial t}\left(n_s\langle\phi\rangle_s\right) + \nabla\cdot\left(n_s\langle\mathbf{u}\phi\rangle_s\right) = n_s\langle\mathbf{a}\cdot\nabla_u\phi\rangle_s + \int \phi\,\omega_s\, d^3u \tag{18}$$

where the relation $\nabla_u\cdot\mathbf{a} = 0$, which follows from Eq. (14), has been used. (Detailed algebra for the derivation of Eq. (18) is presented by Seshadri.[30])

Moments of interest include the mass $\phi = m_s$, momentum $\phi = m_s\mathbf{u}$, and translational kinetic energy $\phi = \frac{1}{2}m_s u^2$ of the particles. Introducing these definitions into Eq. (18), the resulting mass, momentum, and translational energy conservation equations are:

$$\begin{aligned}
\frac{\partial}{\partial t}(n_s m_s) + \nabla\cdot(n_s m_s\langle\mathbf{u}\rangle_s) &= S_s \\
\frac{\partial}{\partial t}(n_s m_s\langle\mathbf{u}\rangle_s) + \nabla\cdot(n_s m_s\langle\mathbf{uu}\rangle_s) &= n_s m_s\langle\mathbf{a}\rangle_s + \mathbf{A}_s \\
\frac{\partial}{\partial t}\left(\tfrac{1}{2}n_s m_s\langle u^2\rangle_s\right) + \nabla\cdot\left(\tfrac{1}{2}n_s m_s\langle\mathbf{u}u^2\rangle_s\right) &= n_s m_s\langle\mathbf{a}\cdot\mathbf{u}\rangle_s + M'_s
\end{aligned} \tag{19}$$

where the source terms due to collisions are:

$$\begin{aligned}
S_s &= m_s\int\omega_s\,d^3u \\
\mathbf{A}_s &= m_s\int\mathbf{u}\,\omega_s\,d^3u \\
M'_s &= \tfrac{1}{2}m_s\int u^2\,\omega_s\,d^3u
\end{aligned} \tag{20}$$

These source terms represent particle generation and destruction by chemical reactions, momentum exchange between fluid species, and kinetic energy exchange in collisions.

Treatment of modes of internal energy, such as rotation, vibration, and electronic excitation, requires some additional work. Let the velocity distribution function associated with particles having internal energy level $\psi_{s\alpha}$ be $f_{s\alpha}$, where the subscript s indicates the species and α indicates the energy level. (The variable α simply represents an enumeration of energy states, and can represent one or more quantum numbers and grouped or ungrouped energy levels.) Define the average over the distribution $f_{s\alpha}$ as $\langle\phi\rangle_{s\alpha} = \int\phi f_{s\alpha}\,d^3u$. The internal energy levels are assumed to be independent of the particle velocity in the sense that $\langle\psi_{s\alpha}\rangle_{s\alpha} = \psi_{s\alpha}$. In analogy to the procedure described above, write the Boltzmann equation for $f_{s\alpha}$, take the moment with $\psi_{s\alpha}$, and sum over all internal energy states. The resulting internal energy equation for species-s is:

$$\frac{\partial}{\partial t}\sum_\alpha n_{s\alpha}\psi_{s\alpha} + \nabla\cdot\sum_\alpha n_{s\alpha}\psi_{s\alpha}\langle\mathbf{u}\rangle_{s\alpha} = M''_s \tag{21}$$

where

$$M''_s = \sum_\alpha\psi_{s\alpha}\int\omega_{s\alpha}\,d^3u \tag{22}$$

Here $n_{s\alpha}$ is the number density of particles having internal energy level $\psi_{s\alpha}$, and $\omega_{s\alpha}$ represents the production rate of particles of internal energy level $\psi_{s\alpha}$ in collisions. Note that $n_s = \sum_\alpha n_{s\alpha}$, $f_s = \sum_\alpha f_{s\alpha}n_{s\alpha}/n_s$, and that the ratio $n_{s\alpha}/n_s$ represents a distribution function for the particles over the possible discrete energy levels. Further, the sum of production rates of particles in each energy state is equal to the production rate for the species as a whole: $\omega_s = \sum_\alpha\omega_{s\alpha}$.

Adding the energy equations (19c) and (21) gives:

$$\begin{aligned}
&\frac{\partial}{\partial t}\left[\sum_\alpha n_{s\alpha}\psi_{s\alpha} + \tfrac{1}{2}n_s m_s\langle u^2\rangle_s\right] \\
&+\nabla\cdot\left[\sum_\alpha n_{s\alpha}\psi_{s\alpha}\langle\mathbf{u}\rangle_{s\alpha} + \tfrac{1}{2}n_s m_s\langle\mathbf{u}u^2\rangle_s\right] = n_s m_s\langle\mathbf{a}\cdot\mathbf{u}\rangle_s + M_s
\end{aligned} \tag{23}$$

Equation (23) is an expression of total energy conservation, and the source term $M_s = M'_s + M''_s$ describes the exchange of total energy between fluid species.

A number of definitions are now introduced to describe the moment terms. The mean velocity is defined

as $\mathbf{v}_s = \langle \mathbf{u} \rangle_s$ and the peculiar velocity as $\mathbf{V}_s = \mathbf{u} - \mathbf{v}_s$. (Note that $\langle \mathbf{V}_s \rangle_s = 0$.) Also defined are the:

$$\begin{aligned}
\text{Kinetic pressure: } & p_s = \tfrac{1}{3} n_s m_s \langle V_s^2 \rangle_s \\
\text{Translational temperature: } & T_s = \tfrac{1}{3} m_s \langle V_s^2 \rangle_s / k_B \\
\text{Thermal energy: } & \epsilon_s = \sum\nolimits_\alpha n_{s\alpha} \psi_{s\alpha} / (n_s m_s) + \tfrac{1}{2} \langle V_s^2 \rangle_s \\
\text{Viscous stress: } & \tau_s = -n_s m_s [\langle \mathbf{V}_s \mathbf{V}_s \rangle_s - \tfrac{1}{3} \langle V_s^2 \rangle_s \mathbf{I}] \\
\text{Heat flux: } & \mathbf{Q}_s = \tfrac{1}{2} n_s m_s \langle \mathbf{V}_s \, V_s^2 \rangle_s + \sum\nolimits_\alpha n_{s\alpha} \psi_{s\alpha} \langle \mathbf{V}_s \rangle_{s\alpha}
\end{aligned} \tag{24}$$

Pressure and temperature are proportional to the average translational kinetic energy of the molecules. Total thermal energy contains a component due to internal energy states as well as translational kinetic energy. Viscous stress is related to the anisotropic component of the velocity correlation, representing transport of momentum by random molecular motions. Similarly, the heat flux represents transport of thermal energy by random molecular motion. Note the additional component of heat flux that arises when particles of a given species in different energy states have different velocity distribution functions.

Using these definitions in Eqs. (19a), (19b), and (23), and introducing the averaged form of (14), the the mass, momentum, and energy conservation equations for species-s become:

$$\begin{aligned}
\frac{\partial \rho_s}{\partial t} + \nabla \cdot (\rho_s \mathbf{v}_s) &= S_s \\
\frac{\partial}{\partial t} (\rho_s \mathbf{v}_s) + \nabla \cdot (\rho_s \mathbf{v}_s \mathbf{v}_s + p_s \mathbf{I}) &= \nabla \cdot \tau_s + \rho_s \mathbf{g} + \zeta_s \left(\mathbf{E} + \mathbf{v}_s \times \mathbf{B} \right) + \mathbf{A}_s \\
\frac{\partial}{\partial t} \left[\rho_s \left(\epsilon_s + \tfrac{1}{2} v_s^2 \right) \right] + \nabla \cdot \left[\rho_s \mathbf{v}_s \left(\epsilon_s + \tfrac{1}{2} v_s^2 \right) + p_s \mathbf{v}_s \right] &= \\
\nabla \cdot [\tau_s \cdot \mathbf{v}_s - \mathbf{Q}_s] + \rho_s \mathbf{v}_s \cdot \mathbf{g} + \zeta_s \mathbf{v}_s \cdot \mathbf{E} + M_s &
\end{aligned} \tag{25}$$

where the mass density has been defined as $\rho_s = n_s m_s$ and the charge density as $\zeta_s = n_s q_s$. Note that the magnetic body force does not appear in Eq. (25c) because $\mathbf{u} \cdot (\mathbf{u} \times \mathbf{B}) = 0$.

Appendix B: Inelastic Collisions

A brief discussion of the form of the inelastic collision source terms is presented here. An alternative treatment is presented in Ch. 7 of Burgers.[23]

For inelastic collisions, the collision term on the right hand side of Eq. (16) can be written in the form:

$$\omega_s = \sum_r R_{rs} \hat{f}_{rs} \tag{26}$$

where R_{rs} is the rate of production or destruction of species-s in the class of inelastic collisions represented by reaction-r, and $\hat{f}_{rs}$ is the distribution function for the subset of particles of species-s participating in reaction-r. Equation (26) is an expression of particle accounting: the rate of generation of particles times the fraction that have a certain velocity gives the rate of change in number of particles in that velocity band.

The reaction rate R_{rs} is a signed quantity, and forward and backward reactions are considered separately. For binary collisions, the particle generation rate has the typical form $R_{rs} = \pm k_r n_a n_b$, where k_r is the rate constant for reaction-r, and n_a and n_b are the number densities of the colliding species.

The distribution function of reacting particles ($\hat{f}_{rs}$) is different from that of the species as a whole (f_s) because only a subset of particles are able to participate in reactions. For example, many reactions have an activation energy threshold, and only particles more energetic than that threshold can react. Similarly, the particles just born in reactions can have a different distribution function from the other members of their species.

Consequently, the reacting particles will have a different mean velocity and a different thermal energy than the species as a whole. Define the average of a property ϕ, with respect to the distribution function

$\hat{f}_{rs}$, as $\langle\phi\rangle_{rs} = \int \phi \hat{f}_{rs}\, d^3u$, and introduce Eq. (26) into Eqs. (20). The following source terms are obtained:

$$\begin{aligned} S_s &= m_s \sum_r R_{rs} \\ \mathbf{A}_s &= m_s \sum_r R_{rs} \langle \mathbf{u} \rangle_{rs} \\ M_s' &= \tfrac{1}{2} m_s \sum_r R_{rs} \langle u^2 \rangle_{rs} \end{aligned} \tag{27}$$

This is again simply particle accounting: the source terms are sums of the particle generation (destruction) rate of species-s times the average mass, momentum, or translational energy the particles appear (disappear) with.

Analogously, let $\omega_{s\alpha} = \sum_r R_{rs\alpha} \hat{f}_{rs\alpha}$, and substitute into Eq. (22). (Note that $R_{rs} = \sum_\alpha R_{rs\alpha}$.) The result is:

$$M_s'' = \sum_r \sum_\alpha R_{rs\alpha} \psi_{s\alpha} \tag{28}$$

This source term is a double summation, over all reactions and internal energy levels, of the rate in reaction-r at which species-s appears in energy level-α times the value of that energy level. Defining $\psi_{rs} = \sum_\alpha R_{rs\alpha} \psi_{s\alpha} / R_{rs}$, indicating how the internal energy of species-s born in reaction-r is distributed over internal energy levels-α, and using (27c) and (28), the total energy source term $M_s = M_s' + M_s''$ can be written as:

$$M_s = \sum_r R_{rs} \left[\psi_{rs} + \tfrac{1}{2} m_s \langle u^2 \rangle_{rs} \right] \tag{29}$$

For the subset of particles-s participating in reaction-r, let $\mathbf{c}_{rs} = \langle \mathbf{u} \rangle_{rs} - \mathbf{v}_s = \langle \mathbf{V}_s \rangle_{rs}$ be the mean velocity relative to the mean flow velocity of all particles of species-s. Similarly, let the difference in internal energy between the reacting particles and the species as a whole be $H_{rs} = \psi_{rs} + \frac{1}{2} m_s \langle V_s^2 \rangle_{rs} - m_s \epsilon_s$. Since both $\mathbf{c}_{rs}$ and H_{rs} are zero if $\hat{f}_{rs} = \hat{f}_{rs\alpha} = f_s$, $\mathbf{c}_{rs}$ will be called the excess velocity and H_{rs} the excess internal energy. Using these definitions in Eqs. (27b) and (29), the inelastic momentum and energy source terms can be rewritten as:

$$\begin{aligned} \mathbf{A}_s &= m_s \sum_r R_{rs} \mathbf{c}_{rs} + S_s \mathbf{v}_s \\ M_s &= \sum_r R_{rs} H_{rs} + m_s \mathbf{v}_s \cdot \sum_r R_{rs} \mathbf{c}_{rs} + S_s \left(\epsilon_s + \tfrac{1}{2} v_s^2 \right) \end{aligned} \tag{30}$$

Note that a minimal, consistent model for the inelastic momentum and energy sources must include at the least the terms proportional to S_s in Eq. (30). Writing the equations in nonconservative form, it becomes apparent that the absence of these terms causes the form of the momentum equation and the thermal energy equation to depend on reference frame, in violation of the principles of classical dynamics and thermodynamics.[33] (The terms containing the excess velocity are invariant because it is a velocity difference.)

Empirical data on reaction rates allow the evaluation of the term S_s in (27a). A precise model of the momentum and energy terms in (30) would require specific information on the distribution functions of the reacting particles. Some reasonable assumptions, however, can be made to create a closure model for these terms: the excess velocity will be assumed to be negligible ($\mathbf{c}_{rs} \approx 0$), and the excess internal energy H_{rs} of the reacting species will be approximated by the equilibrium heat of reaction per particle.

Using $\mathbf{c}_{rs} \approx 0$, the inelastic collision source terms for each species-s of charged particle are:

$$\begin{aligned} S_s &= m_s \sum_r R_{rs} \\ \mathbf{A}_s &= S_s \mathbf{v}_s \\ M_s &= \sum_r R_{rs} H_{rs} + S_s \left(\epsilon_s + \tfrac{1}{2} v_s^2 \right) \end{aligned} \tag{31}$$

Empirical data can be used for the reaction rates and the heat of reaction. The error incurred in the momentum term by neglecting the excess velocity may be mitigated by an appropriately chosen collision frequency, taken from experimental data, in the elastic collision terms.

Appendix C: Elastic Collisions

A more complete theoretical treatment is available for the elastic collisions,[23] based on the BGK model.[34] The model used for the term ω_s has the same form as Eq. (26), but in the form of paired interactions. All particles entering collisions are assumed to participate equally, so those particles have the same distribution function f_s as the species as a whole. Particles coming out of collisions are assumed to have completely randomized velocities, and have a distribution f^*_{st} with local mean velocity $\mathbf{v}_{st}$ and temperature T_{st}. (This notation represents particles of species-s coming out of collisions with species-t.) The form of the Boltzmann equation source term is then:

$$\omega_s = \sum_t k_{st} n_s n_t (f^*_{st} - f_s) \tag{32}$$

where the sum includes the case $t = s$, and the rate parameter k_{st} is taken to be independent of particle velocity. The resulting moment equation source terms, analogous to Eq. (27), are:

$$\begin{aligned} S_s &= 0 \\ \mathbf{A}_s &= m_s n_s \sum_t k_{st} n_t (\mathbf{v}_{st} - \mathbf{v}_s) \\ M'_s &= \tfrac{1}{2} m_s n_s \sum_t k_{st} n_t \left[\frac{3k_B}{m_s} (T_{st} - T_s) + v^2_{st} - v^2_s \right] \end{aligned} \tag{33}$$

where the relations $\langle \mathbf{u} \rangle_{st} = \mathbf{v}_{st}$ and $\langle u^2 \rangle_{st} = v^2_{st} + 3k_B T_{st}/m_s$ have been used.

The variables $\mathbf{v}_{st}$ and T_{st} must now be related to the other flow variables. To do this, we use the fact that mass, momentum, and kinetic energy are conserved in an elastic collision. We assume that particle velocities are fully randomized in collisions, so there is no preferential direction for the particles exiting a collision, and the particle velocities entering and leaving the collision are all uncorrelated. The mean velocity coming out of a collision is then:

$$\mathbf{v}_{st} = \frac{m_s \mathbf{v}_s + m_t \mathbf{v}_t}{m_s + m_t} \tag{34}$$

and the corresponding mean thermal energy is:

$$\tfrac{3}{2} k_B T_{st} = \tfrac{3}{2} k_B T_s + \frac{m_{st}}{m_s + m_t} \left[3k_B (T_t - T_s) + \tfrac{1}{2} m_t |\mathbf{v}_t - \mathbf{v}_s|^2 \right] \tag{35}$$

where $m_{st} = m_s m_t / (m_s + m_t)$ is the reduced mass. Introducing Eqs. (34) and (35) into Eqs. (33), and simplifying, we arrive at the model used here for momentum and energy exchange in elastic collisions:

$$\begin{aligned} \mathbf{A}_s &= -n_s \sum_t m_{st} \nu_{st} (\mathbf{v}_s - \mathbf{v}_t) \\ M_s &= -n_s \sum_t \frac{m_{st} \nu_{st}}{m_s + m_t} \left[3k_B (T_s - T_t) + (\mathbf{v}_s - \mathbf{v}_t) \cdot (m_s \mathbf{v}_s + m_t \mathbf{v}_t) \right] \end{aligned} \tag{36}$$

Here $\nu_{st} = k_{st} n_t$ is the average momentum transfer collision frequency between particles of types s and t.

Acknowledgments

This project is sponsored in part by the Air Force Office of Scientific Research (monitored by F. Fahroo), and by a grant of High Performance Computing time from the Air Force Research Laboratory Major Shared Resource Center. The author would like to acknowledge helpful discussions of this ongoing project with his colleagues D. Gaitonde and M. White, and with visiting summer faculty G. Font and R. Lilly.

References

[1] Lieberman, M. A. and Lichtenberg, A. J., *Principles of Plasma Discharges and Materials Processing*, J. Wiley, New York, 1994.

[2] Fridman, A. and Kennedy, L. A., *Plasma Physics and Engineering*, Taylor and Francis, New York, 2004.

[3] Roupassov, D. V., Nikipelov, A. A., Nudnova, M. M., and Starikovskii, A. Y., "Flow Separation Control by Plasma Actuator with Nanosecond Pulsed-Periodic Discharge," *AIAA Journal*, Vol. 47, No. 1, 2009, pp. 168–185.

[4]Bredan, D. and Raja, L. L., "Simulations of Nanosecond Pulsed Plasmas in Supersonic Flow," AIAA Paper 2009-3594, June 2009.

[5]Likhanskii, A. V., Semak, V. V., Shneider, M. N., Opaits, D. F., Miles, R. B., and Macheret, S. O., "The Role of the Photoionization in the Numerical Modeling of the DBD Plasma Actuator," AIAA Paper 2009-841, January 2009.

[6]Murray, R. C., Zaidi, S. H., Carraro, M. R., Vasilyak, L. M., Macheret, S. O., Shneider, M. N., and Miles, R. B., "Magnetohydrodynamic Power Generation Using Externally Ionized, Cold, Supersonic Air as Working Fluid," *AIAA Journal*, Vol. 44, No. 1, 2006, pp. 119–127.

[7]Adamovich, I. V., Lempert, W. R., Nishihara, M., Rich, J. W., and Utkin, Y. G., "Repetitively Pulsed Nonequilibrium Plasmas for Magnetohydrodynamic Flow Control and Plasma-Assisted Combustion," *Journal of Propulsion and Power*, Vol. 24, No. 6, 2008, pp. 1198–1215.

[8]Font, G. I., "Boundary-Layer Control with Atmospheric Plasma Discharges," *AIAA Journal*, Vol. 44, No. 7, 2006, pp. 1572–1578.

[9]Ward, A. L., "Calculations of Cathode-Fall Characteristics," *Journal of Applied Physics*, Vol. 33, No. 9, 1962, pp. 2789–2794.

[10]Boeuf, J.-P., "A Two-Dimensional Model of DC Glow Discharges," *Journal of Applied Physics*, Vol. 63, No. 5, 1988, pp. 1342–1349.

[11]Raizer, Y. P. and Surzhikov, S. T., "Two-Dimensional Structure in a Normal Glow Discharge and Diffusion Effects in Cathode and Anode Spot Formation," *High Temperature*, Vol. 26, No. 3, 1988, pp. 304–311.

[12]Graves, D. B. and Jensen, K. F., "A Continuum Model of DC and RF Discharges," *IEEE Transactions on Plasma Science*, Vol. PS-14, No. 2, 1986, pp. 78–91.

[13]Passchier, J. D. P. and Goedheer, W. J., "A Two-Dimensional Fluid Model for an Argon RF Discharge," *Journal of Applied Physics*, Vol. 74, No. 6, 1993, pp. 3744–3751.

[14]Young, F. F., "Two-Dimensional, Self-Consistent, Three-Moment Simulation of RF Glow Discharges," *IEEE Transactions on Plasma Science*, Vol. 21, No. 3, 1993, pp. 312–321.

[15]Meyyappan, M. and Kreskovsky, J. P., "Glow Discharge Simulation Through Solutions to the Moments of the Boltzmann Transport Equation," *Journal of Applied Physics*, Vol. 68, No. 4, 1990, pp. 1506–1512.

[16]Meyyappan, M., "A Continuum Model for Low-Pressure Radio-Frequency Discharges," *Journal of Applied Physics*, Vol. 69, No. 12, 1991, pp. 8047–8051.

[17]Meyyappan, M. and Govindan, T. R., "Two-Dimensional Analysis of Radio Frequency Discharges," *IEEE Transactions on Plasma Science*, Vol. 24, No. 1, 1996, pp. 119–120.

[18]Wilcoxson, M. H. and Manousiouthakis, V. I., "Simulation of a Three-Moment Fluid Model of a Two-Dimensional Radio Frequency Discharge," *Chemical Engineering Science*, Vol. 51, No. 7, 1996, pp. 1089–1106.

[19]D'Ambrosio, D. and Giordano, D., "Electromagnetic Fluid Dynamics for Aerospace Applications," *Journal of Thermophysics and Heat Transfer*, Vol. 21, No. 2, 2007, pp. 284–302.

[20]MacCormack, R. W., "Solution of Maxwell's Equations Coupled to the Navier-Stokes Equations," AIAA Paper 2009-3911, June 2009.

[21]Hakim, A. and Shumlak, U., "Two-Fluid Physics and Field-Reversed Configurations," *Physics of Plasmas*, Vol. 14, No. 5, 2007, pp. 055911–1 – 055911–11.

[22]Park, S.-K. and Economou, D. J., "Analysis of Low Pressure RF Glow Discharges Using Continuum Model," *Journal of Applied Physics*, Vol. 68, No. 8, 1990, pp. 3904–3915.

[23]Burgers, J. M., *Flow Equations for Composite Gases*, Academic Press, New York, 1969.

[24]White, F. M., *Viscous Fluid Flow*, McGraw-Hill, New York, 2nd ed., 1991.

[25]Hoffmann, K. A. and Chiang, S. T., *Computational Fluid Dynamics*, Engineering Educational System, Wichita KS, 4th ed., 2000.

[26]Anderson, W. K., Thomas, J. L., and van Leer, B., "A Comparison of Finite Volume Flux Vector Splittings for the Euler Equations," AIAA Paper 85-0122, January 1985.

[27]Cheney, W. and Kincaid, D., *Numerical Mathematics and Computing*, Brooks/Cole Publishing, Pacific Grove, California, 3rd ed., 1994.

[28]Graves, D. B., "Fluid Model Simulations of a 13.56-MHz RF Discharge: Time and Space Dependence of Rates of Electron Impact Ionization," *Journal of Applied Physics*, Vol. 62, No. 1, 1987, pp. 88–94.

[29]Chapman, S. and Cowling, T. G., *The Mathematical Theory of Non-Uniform Gases*, Cambridge University Press, 2nd ed., 1952.

[30]Seshadri, S. R., *Fundamentals of Plasma Physics*, Elsevier, New York, 1973.

[31]Olejniczak, J. and Candler, G. V., "Vibrational Energy Conservation with Vibration-Dissociation Coupling: General Theory and Numerical Studies," *Physics of Fluids*, Vol. 7, No. 7, 1995, pp. 1764–1774.

[32]Hirschfelder, J. O., Curtis, C. F., and Bird, R. B., *Molecular Theory of Gases and Liquids*, J. Wiley, New York, 1954.

[33]Lam, S. H., "MAE 558: Plasmadynamics Notes," Department of Mechanical and Aerospace Engineering, Princeton University, Princeton NJ 08544. URL: http://www.princeton.edu/∼lam/SHL/Plasma.pdf [accessed 3 June 2008].

[34]Bhatnagar, P. L., Gross, E. P., and Krook, M., "A Model for Collision Processes in Gasses. I. Small Amplitude Processes in Charged and Neutral One-Component Systems," *Physical Review*, Vol. 94, No. 3, 1954, pp. 511–525.

	Inflow ($v_e^\perp < 0$)	Outflow ($v_e^\perp > 0$)
Subsonic ($\lvert v_e^\perp \rvert < a_e$)	extrapolate n_e $v_e^\perp = k_r - \gamma_E \Gamma_i^+ / n_e$ $\mathbf{v}_e^\parallel = 0$ $T_e = \text{avg}(T_{ea}, T_{es})$	extrapolate n_e $v_e^\perp = k_r - \gamma_E \Gamma_i^+ / n_e$ extrapolate $\mathbf{v}_e^\parallel$ $T_e = \text{avg}(T_{ea}, T_{es})$
Supersonic ($\lvert v_e^\perp \rvert \geq a_e$)	$n_e = \gamma_E \Gamma_i^+ / a_e$ $v_e^\perp = -a_e$ $\mathbf{v}_e^\parallel = 0$ $T_e = T_{es}$	extrapolate n_e extrapolate $\mathbf{v}_e$ extrapolate T_e

(a) Electrons, five-moment model.

Inflow ($v_i^\perp < 0$)	Outflow ($v_i^\perp > 0$)
extrapolate n_i $v_i^\perp = 0$ extrapolate $\mathbf{v}_i^\parallel$ $T_i = T_\infty$	extrapolate n_i extrapolate $\mathbf{v}_i$ extrapolate T_i

(b) Ions, five-moment model.

Inflow/Outflow
$n_e v_e^\perp = n_e k_r - \gamma_E n_i v_i^+$ $T_e = \text{avg}(T_{ea}, T_{es})$

(c) Electrons, two-moment model.

Inflow ($v_i^\perp < 0$)	Outflow ($v_i^\perp > 0$)
$v_i^\perp = 0$ $T_i = T_\infty$	extrapolate n_i extrapolate T_i

(d) Ions, two-moment model.

Figure 1. Boundary conditions for charged particles.

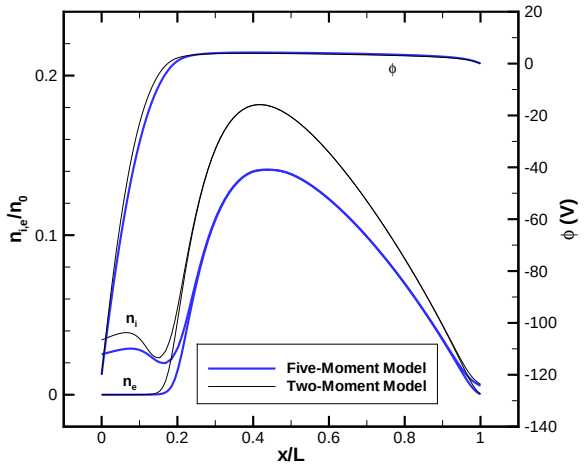

(a) Number densities and potential.

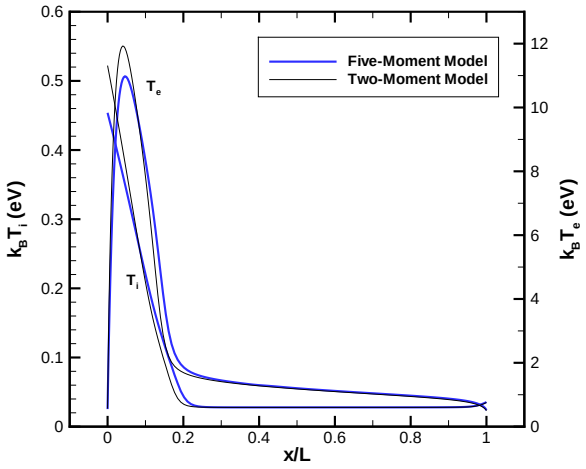

(b) Temperatures.

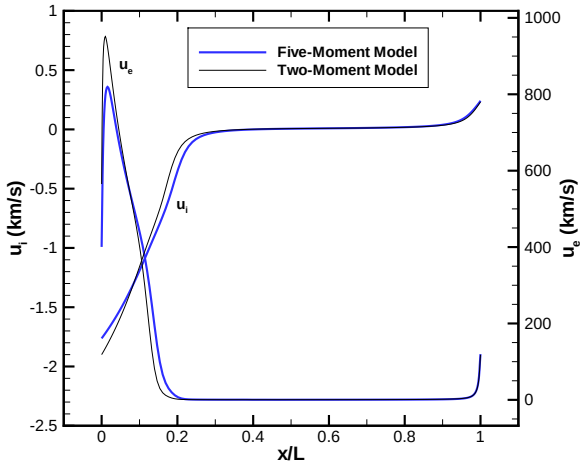

(c) Velocities.

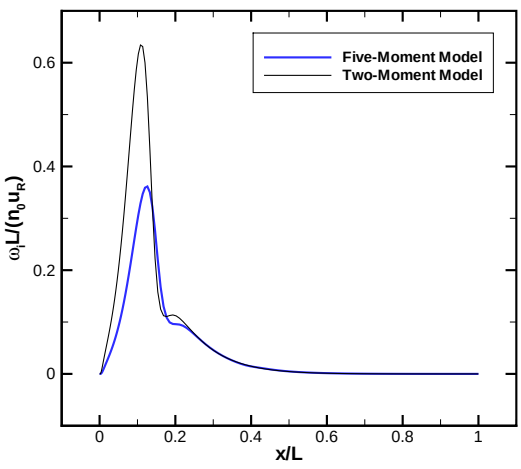

(d) Ionization rate.

Figure 2. Comparison of two-moment and five-moment models for one-dimensional, DC discharge.

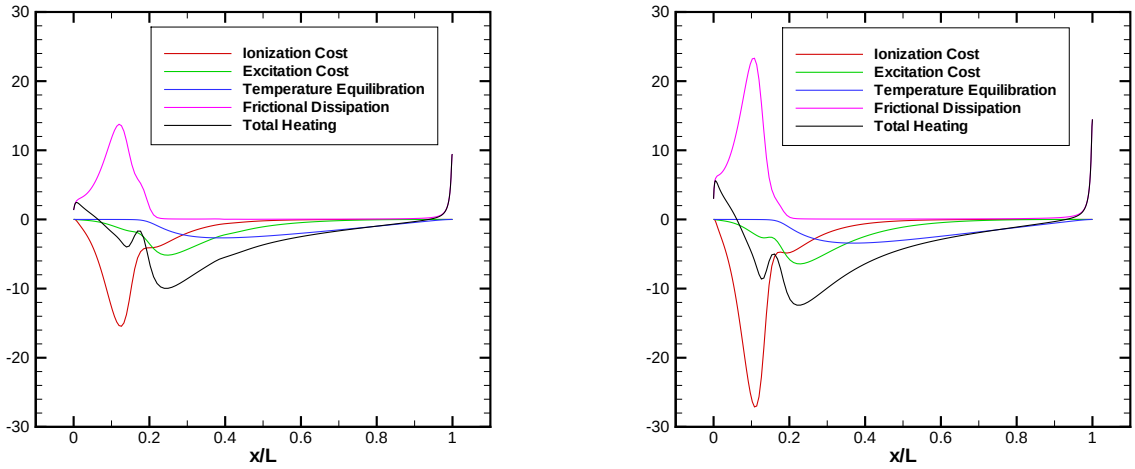

(a) Five-moment model. (b) Two-moment model.

Figure 3. Electron heating terms for one-dimensional, DC discharge.

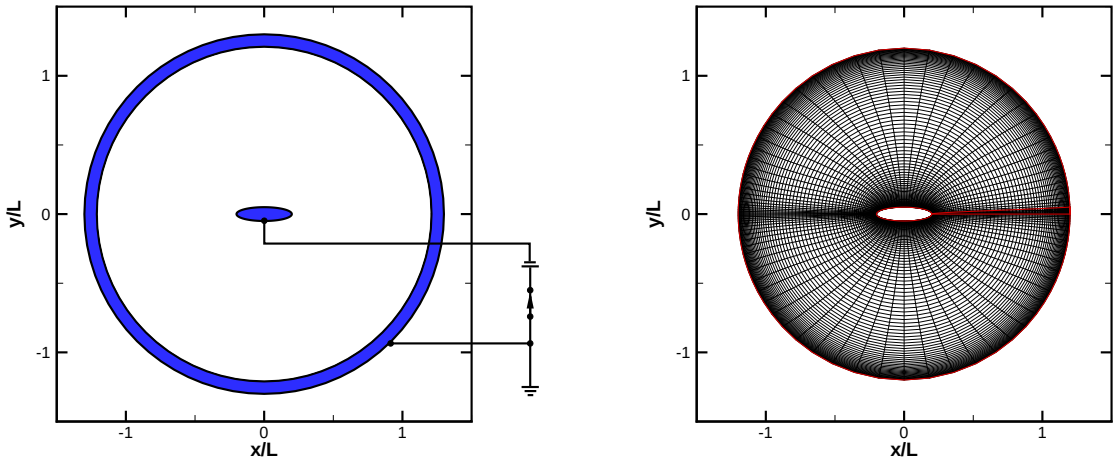

(a) Schematic diagram. (b) Computational mesh.

Figure 4. Transient discharge problem with elliptical cathode.

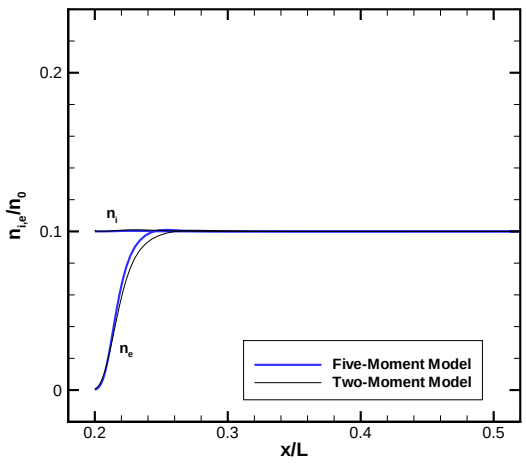

(a) Number density.

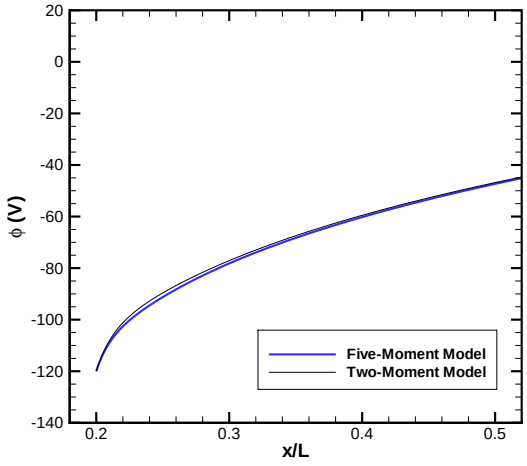

(b) Potential.

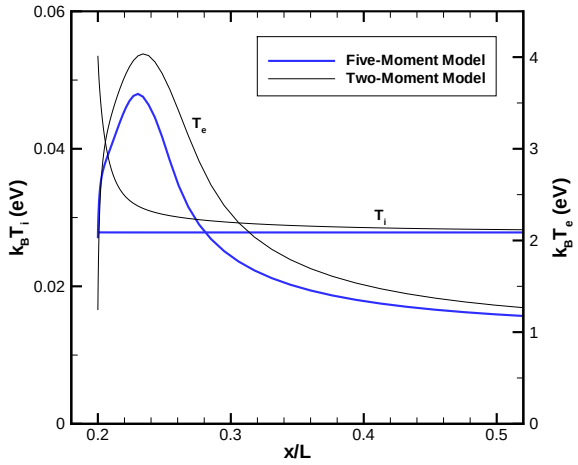

(c) Temperature.

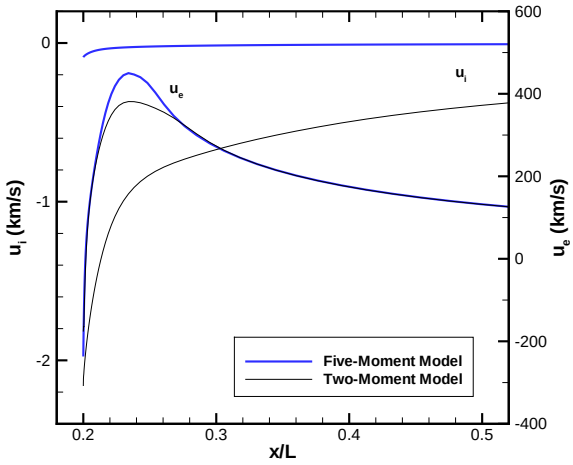

(d) Horizontal velocity component.

Figure 5. Cathode sheath evolution in transient discharge (1 ns).

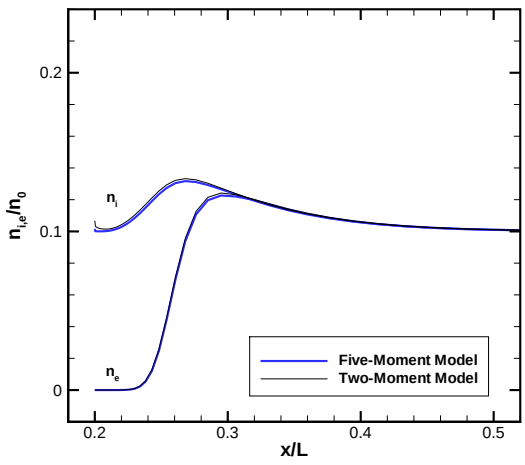

(a) Number density.

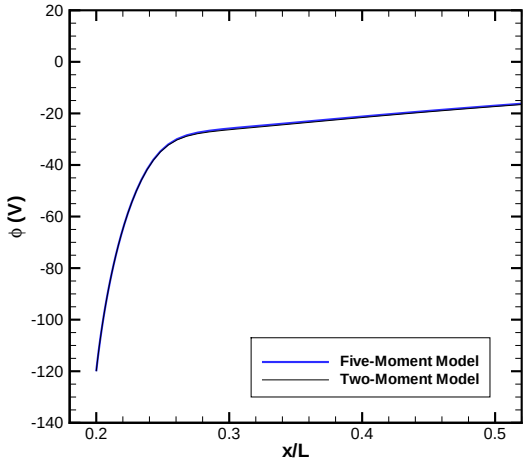

(b) Potential.

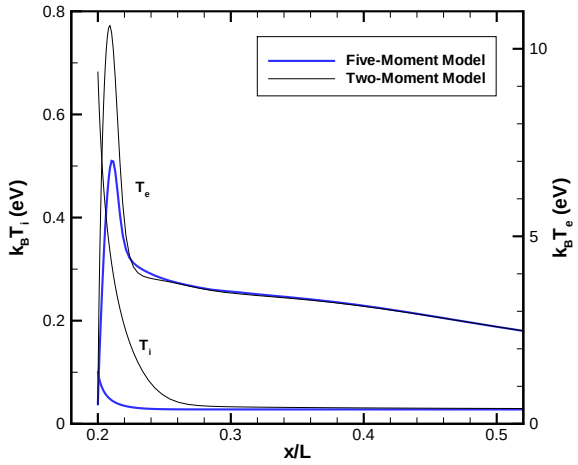

(c) Temperature.

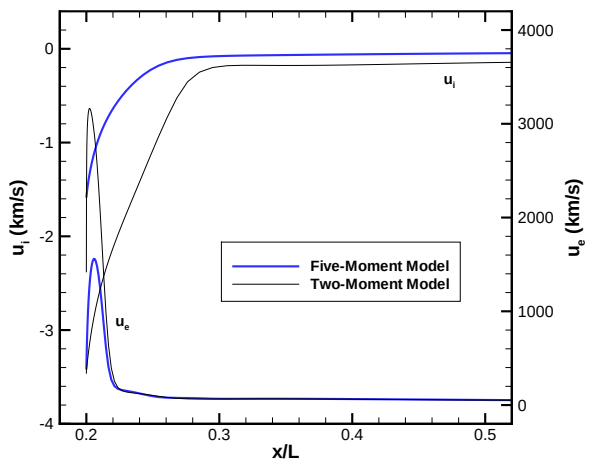

(d) Horizontal velocity component.

Figure 6. Cathode sheath evolution in transient discharge (10 ns).

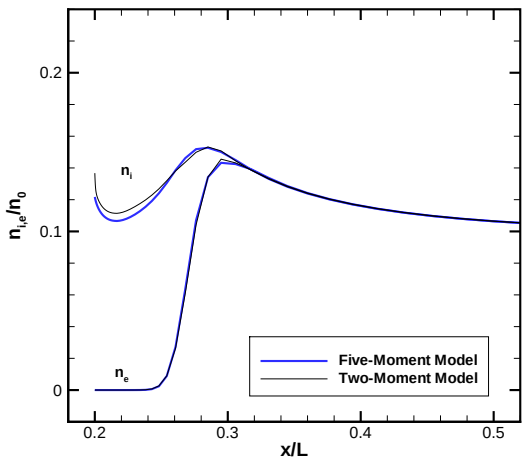

(a) Number density.

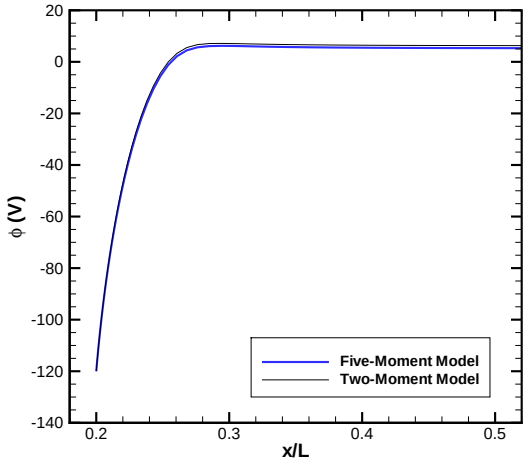

(b) Potential.

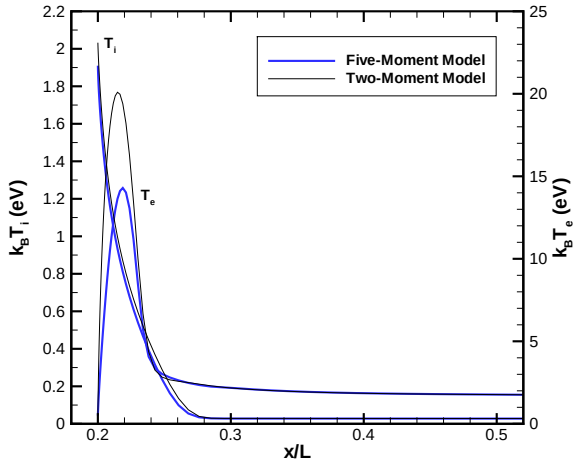

(c) Temperature.

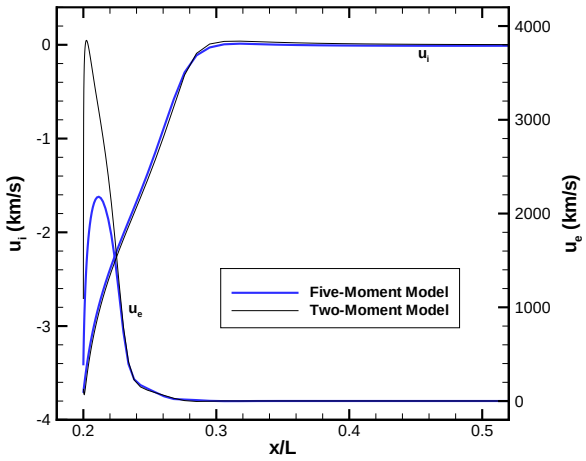

(d) Horizontal velocity component.

Figure 7. Cathode sheath evolution in transient discharge (100 ns).

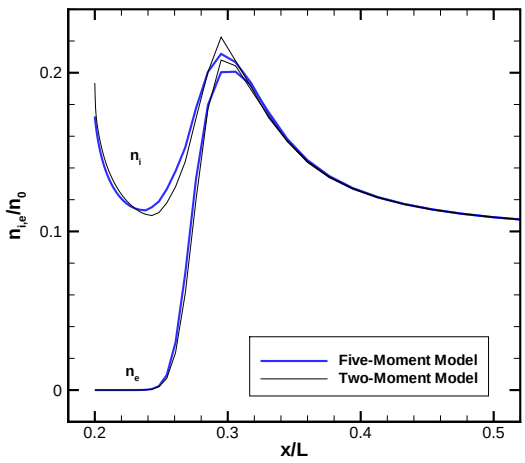

(a) Number density.

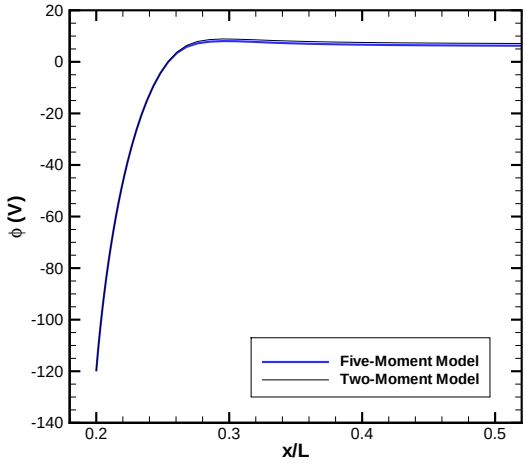

(b) Potential.

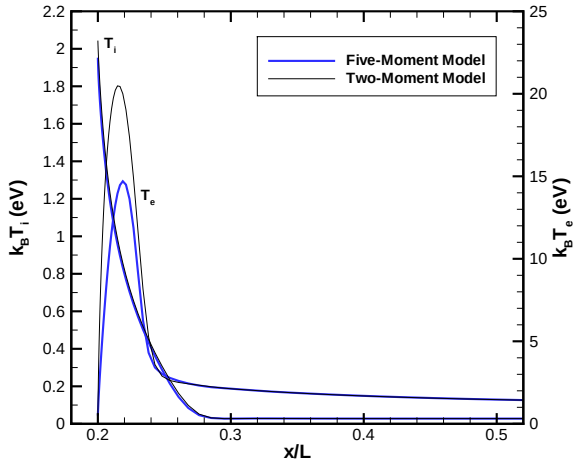

(c) Temperature.

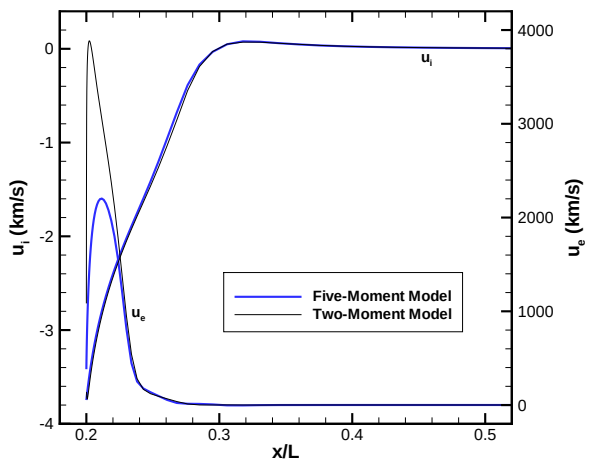

(d) Horizontal velocity component.

Figure 8. Cathode sheath evolution in transient discharge (1000 ns).

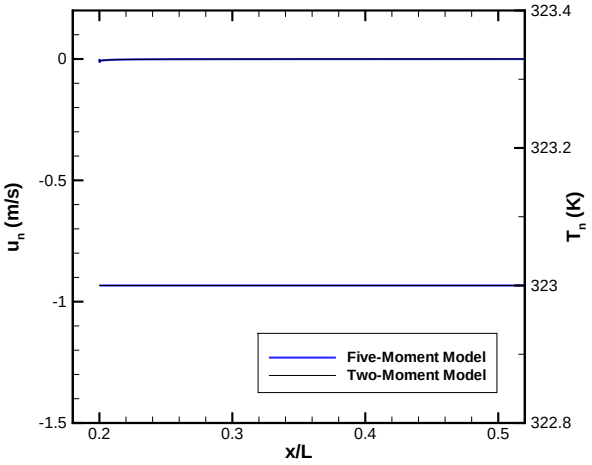

(a) 1 ns.

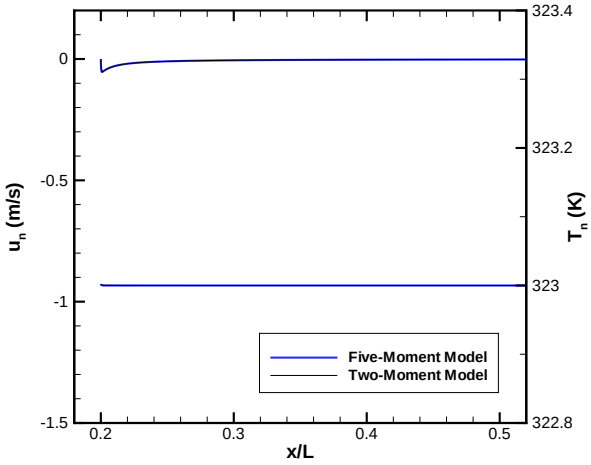

(b) 10 ns.

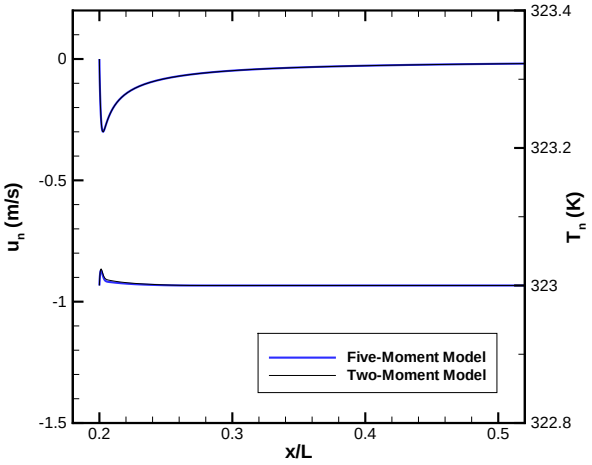

(c) 100 ns.

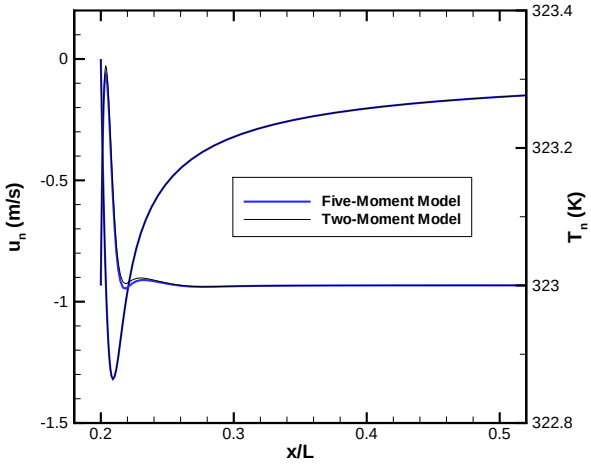

(d) 1000 ns.

Figure 9. Horizontal velocity component and temperature for neutral particles.

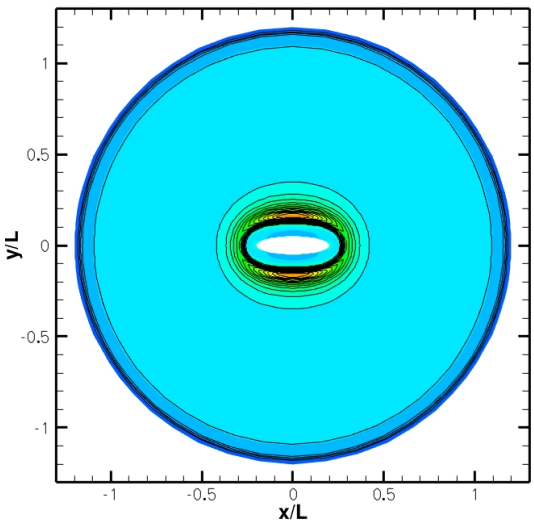

(a) Number densities (contour 2×10^{13} m^{-3}).

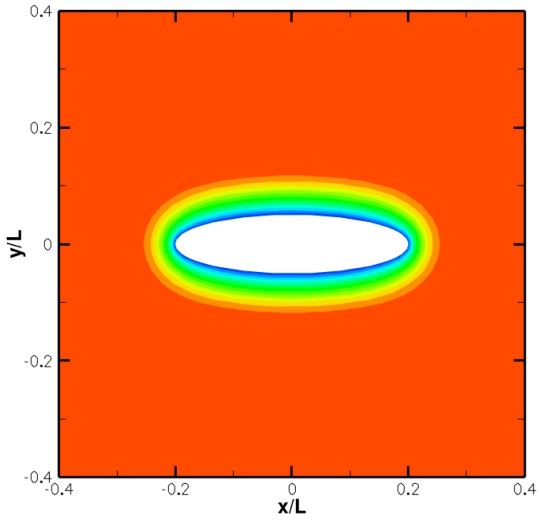

(b) Potential (contour 10 V).

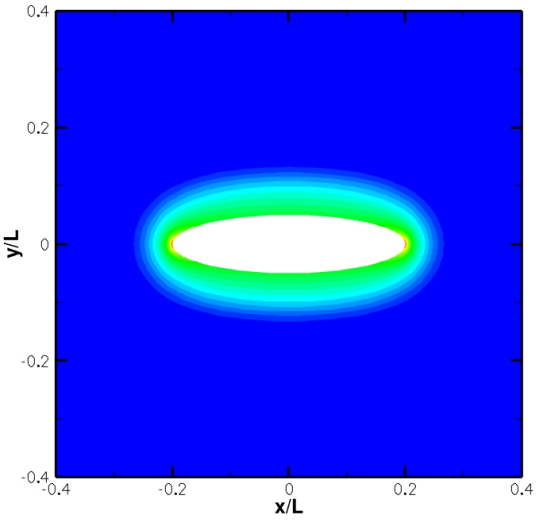

(c) Ion temperature (contour 0.1 eV).

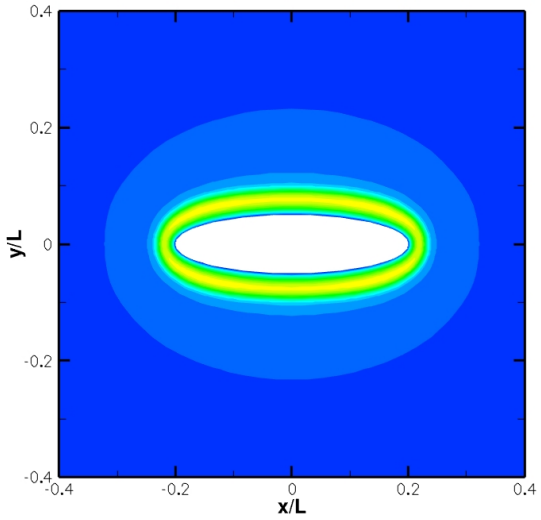

(d) Electron temperature (contour 1 eV).

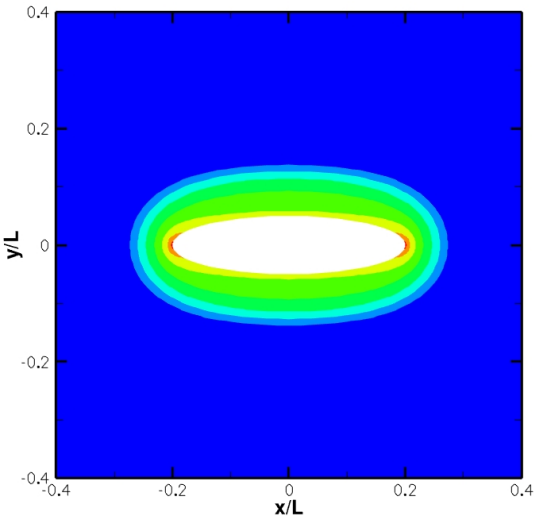

(e) Ion speed (contour 0.5 km/s).

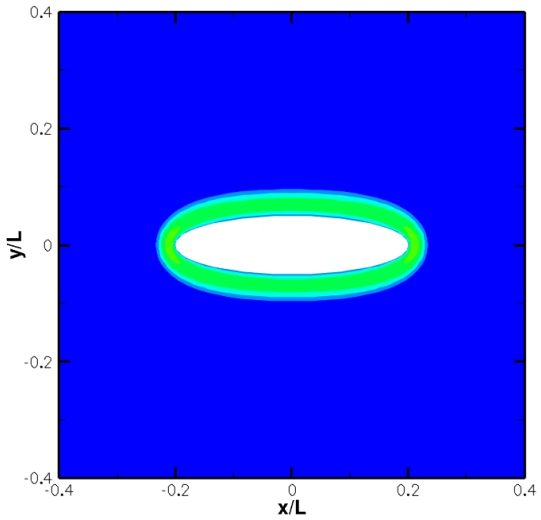

(f) Electron speed (contour 500 km/s).

Figure 10. Results for transient elliptic cathode problem, five-moment model (1000 ns).

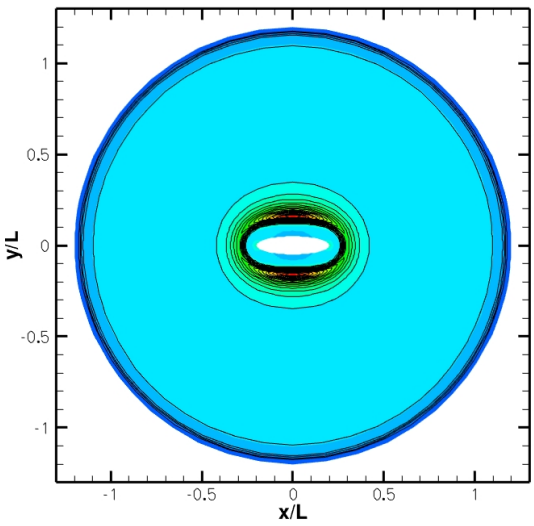

(a) Number densities (contour 2×10^{13} m^{-3}).

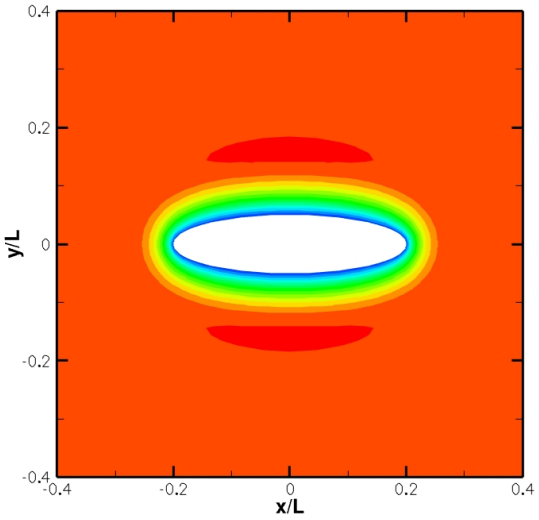

(b) Potential (contour 10 V).

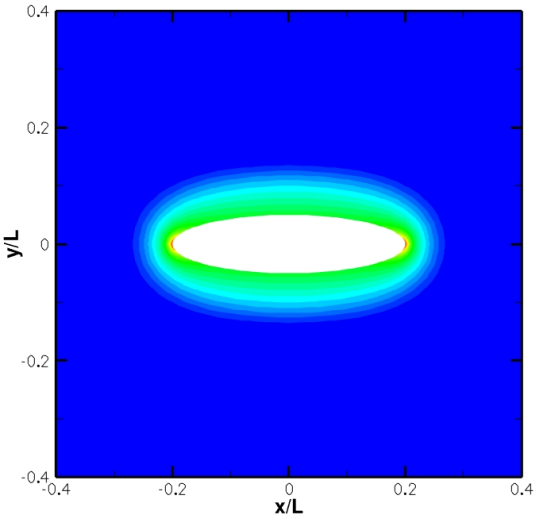

(c) Ion temperature (contour 0.1 eV).

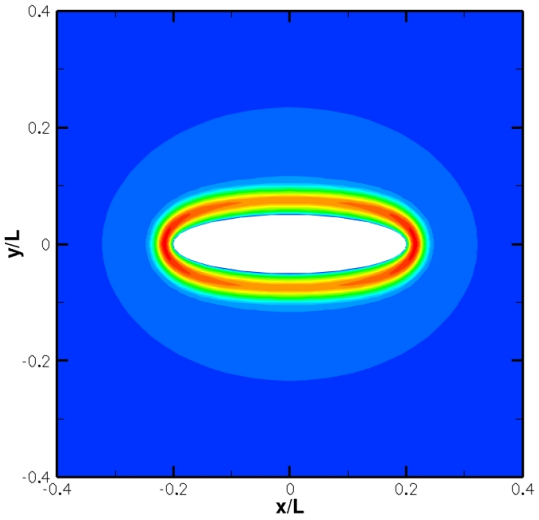

(d) Electron temperature (contour 1 eV).

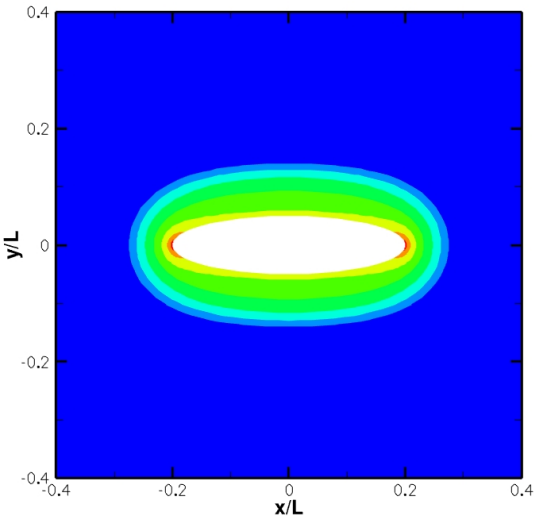

(e) Ion speed (contour 0.5 km/s).

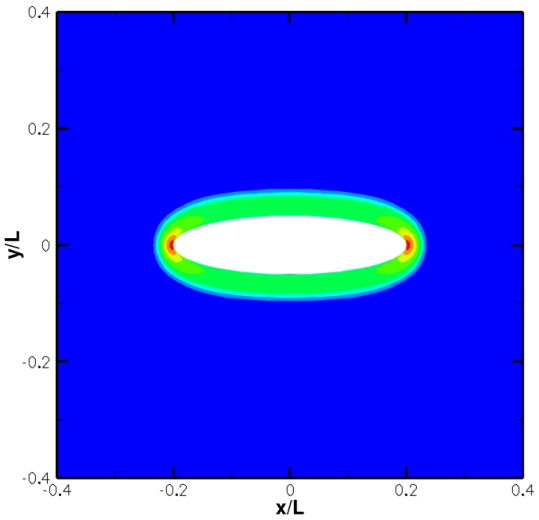

(f) Electron speed (contour 500 km/s).

Figure 11. Results for transient elliptic cathode problem, two-moment model (1000 ns).

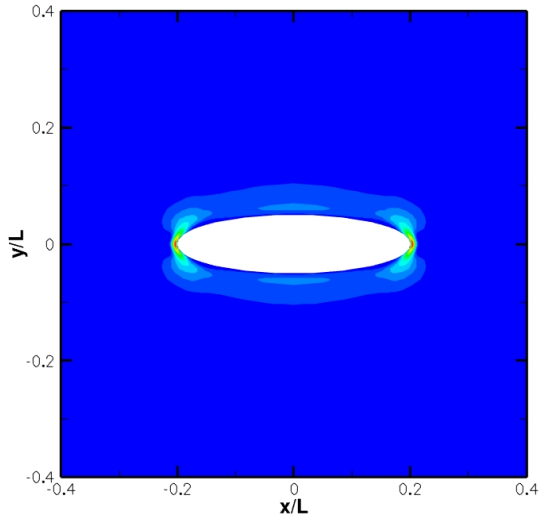

(a) Neutral temperature, 5-moment model (contour 0.02 K).

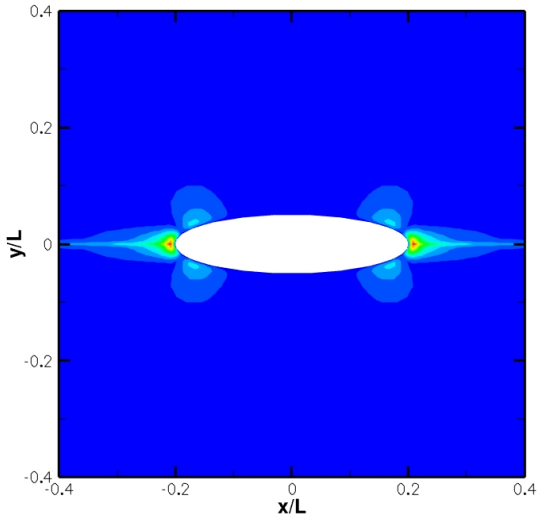

(b) Neutral speed, 5-moment model (contour 0.1 m/s).

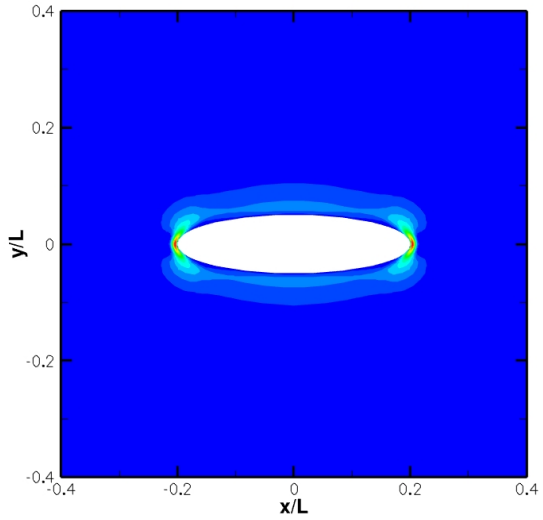

(c) Neutral temperature, 2-moment model (contour 0.02 K).

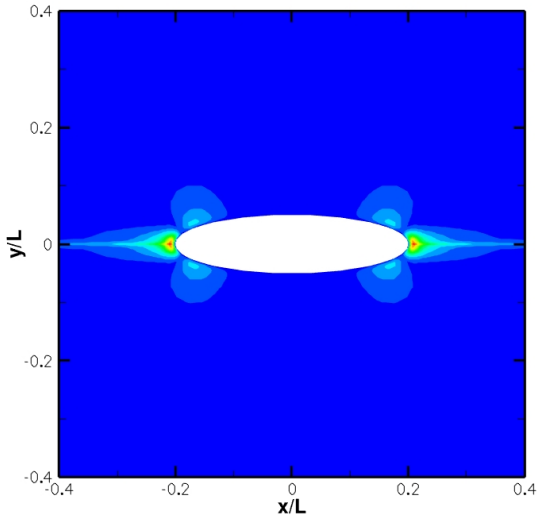

(d) Neutral speed, 2-moment model (contour 0.1 m/s).

Figure 12. Neutral particle properties in transient elliptic cathode problem (1000 ns).